AGU PUBLICATIONS

JGR

Journal of Geophysical Research: Atmospheres

RESEARCH ARTICLE
10.1002/2017JD026515

Key Points:
- Passive microwave method (Peterson et al., 2015) applied to global satellite data provides best agreement with measured diurnal variation
- Including conductivity profile from global circulation model CESM decreases peak to peak diurnal variation from 24% to 20% due to clouds
- Proper method to use conductivity from CESM within 3-D GEC models is suggested

Correspondence to:
J. Jánský,
jxj21@psu.edu

Citation:
Jánský, J., Lucas, G. M., Kalb, C., Bayona, V., Peterson, M. J., Deierling, W., … Pasko, V. P. (2017). Analysis of the diurnal variation of the global electric circuit obtained from different numerical models. *Journal of Geophysical Research: Atmospheres*, *122*, 12,906–12,917. https://doi.org/10.1002/2017JD026515

Received 16 JAN 2017
Accepted 7 NOV 2017
Accepted article online 13 NOV 2017
Published online 7 DEC 2017

Analysis of the Diurnal Variation of the Global Electric Circuit Obtained From Different Numerical Models

Jaroslav Jánský[1], Greg M. Lucas[2], Christina Kalb[3], Victor Bayona[4], Michael J. Peterson[3], Wiebke Deierling[2], Natasha Flyer[4], and Victor P. Pasko[1]

[1]Communications and Space Sciences Laboratory, Department of Electrical Engineering, Penn State University, University Park, PA, USA, [2]Department of Aerospace Engineering Sciences, University of Colorado Boulder, Boulder, CO, USA, [3]National Center for Atmospheric Research, Boulder, CO, USA, [4]Institute for Mathematics Applied to Geosciences, National Center for Atmospheric Research, Boulder, CO, USA

Abstract This work analyzes different current source and conductivity parameterizations and their influence on the diurnal variation of the global electric circuit (GEC). The diurnal variations of the current source parameterizations obtained using electric field and conductivity measurements from plane overflights combined with global Tropical Rainfall Measuring Mission satellite data give generally good agreement with measured diurnal variation of the electric field at Vostok, Antarctica, where reference experimental measurements are performed. An approach employing 85 GHz passive microwave observations to infer currents within the GEC is compared and shows the best agreement in amplitude and phase with experimental measurements. To study the conductivity influence, GEC models solving the continuity equation in 3-D are used to calculate atmospheric resistance using yearly averaged conductivity obtained from the global circulation model Community Earth System Model (CESM). Then, using current source parameterization combining mean currents and global counts of electrified clouds, if the exponential conductivity is substituted by the conductivity from CESM, the peak to peak diurnal variation of the ionospheric potential of the GEC decreases from 24% to 20%. The main reason for the change is the presence of clouds while effects of ^{222}Rn ionization, aerosols, and topography are less pronounced. The simulated peak to peak diurnal variation of the electric field at Vostok is increased from 15% to 18% from the diurnal variation of the global current in the GEC if conductivity from CESM is used.

1. Introduction

The global electric circuit (GEC) is established by the naturally occurring presence of a thin veneer of insulating air (our atmosphere) sandwiched between the highly conducting Earth and the ionosphere (e.g., Williams, 2009). Wilson (1921) first suggested that thunderstorms and electrified shower clouds, called together electrified clouds, are the main generators in the GEC responsible for maintaining the potential difference of approximately 240 kV (e.g., Markson, 2007). In "fair-weather" regions, away from generators, a current density of several picoamperes per square meter flows from the ionosphere to the ground and a vertical electric field between 100 and 300 V m^{-1} can be measured near ground level (Burns et al., 2012). During the first quarter of the twentieth century, the Carnegie Institution of Washington operated survey ships, which made hourly measurements of the atmospheric electric field in oceanic air (e.g., Harrison, 2013, and references therein). The measurements suggested that the diurnal field variation in universal time was independent of the ship's position and that it is a key part of the understanding of the GEC (Aplin et al., 2008; Harrison, 2013). Recent measurements of the electric field on the Antarctic plateau complement and improve the accuracy and understanding of the diurnal variation of the electric field near the ground (Burns et al., 2012, 2015). The Antarctic plateau provides advantages that appear useful for long-term as well as short-term measurements of the atmospheric global circuit: it is distant from major sources of natural and anthropogenic aerosols, no local biological activity, atmospheric water vapor content is minimal, and wind-induced variations in conductivity associated with natural radioactivity are absent (Burns et al., 2012).

The relation of the diurnal variation of the electric field near the ground with electrified clouds was first examined by Whipple (1929) and Whipple and Scrase (1936). It was found that worldwide thunder day statistics

produced a curve with similar phase, but incorrect amplitude. Mach et al. (2011) combined the analysis of high-altitude aircraft observations of electrified clouds with diurnal lightning statistics (Bailey et al., 2007). Using basic assumptions about the mean storm currents as a function of flash rate and location (i.e., land or ocean), a very good agreement in amplitude with the diurnal variation of the surface electric field was achieved. Liu et al. (2010) utilized 10 years of Tropical Rainfall Measuring Mission (TRMM) observations. The global diurnal variation of rainfall, the raining area from thunderstorms, and electrified shower clouds were derived and provided a better match to the diurnal variation of the surface electric field than that obtained by Whipple (1929).

Numerical modeling of GEC complements the experimental measurements and serves to provide better understanding of physical mechanisms recently reviewed in (e.g., Williams & Mareev, 2014). Numerical models are useful for creating the forecasts of the expected electrical conditions. Recently, Mareev and Volodin (2014) used the general circulation model INMCM4.0 for modeling of GEC, and forecasting ionospheric potential and lightning flash rate. The parameterization of ionospheric potential (Kalinin et al., 2011) was utilized, which takes into account quasi-stationary currents of electrified clouds, determined from areas where convection arises in INMCM4.0, as principal contributors to the GEC. Mareev and Volodin (2014) evaluated the diurnal variation of the ionospheric potential and suggested to study GEC with more realistic conductivity model. Another global circulation model, specifically the Community Earth System Model (CESM), has recently been extended to provide a calculation of conductivity in the troposphere and stratosphere (Baumgaertner et al., 2013, 2014). Lucas et al. (2015) utilized CESM including global conductivity and developed a new modeling framework of the GEC for use within CESM that is called Whole Atmosphere Community Climate Model (WACCM)-GEC. This framework utilizes current source distributions based on parameterization of convective mass flux (Kalb et al., 2016). Convective mass flux is a quantity from CESM, which correlates best with electric currents above thunderstorms (Kalb et al., 2016).

The motivation for present work is to model and compare the diurnal variation of the GEC using several different modeling strategies for current source parameterizations and to analyze the influence of conductivity, obtained from CESM, on the diurnal variation. Bayona et al. (2015) developed a three-dimensional GEC model with ability to incorporate topography with very high precision and described two methods for incorporating current sources due to electrified clouds into the model. For the first method, the sources are input as current dipoles with each dipole representing an electrified cloud. This method is used to study the effects of the global conductivity distribution obtained from CESM on the diurnal variation of the global current and ionospheric potential of the GEC. Second, the sources are input as current density distributions at a fixed altitude above the electrified clouds. Two methods (Kalb et al., 2014; Peterson et al., 2015) of obtaining the global current distribution at 20 km come from a combination of local measurements obtained from plane overflights (either current density or 85 GHz passive microwave observations) with global satellite data (either thunderstorm and electrified shower cloud counts or 85 GHz passive microwave observations) and two methods (Kalb et al., 2016; Lucas et al., 2015) utilizing the global circulation model CESM are used. There is a connection between the models, as data from (Kalb et al., 2014) were used for calibration of parameterization of current at 20 km using convective mass flux, which can be obtained from models like CESM (Kalb et al., 2016), and Lucas et al. (2015) used CESM with a parametrization of current (Kalb et al., 2016). The model of Lucas et al. (2015) is used to quantify the effect of conductivity in the fair-weather part of the GEC. This conductivity, obtained from CESM, has an effect on the diurnal variation of the electric field at Vostok, where corresponding experimental measurements were made (Burns et al., 2012).

The specific goal of the present work is to conduct a comparison of performances of previously developed models when these are executed under similar conditions. The annual average of diurnal variation is selected as a common line for comparison in present work. It is important to note that the diurnal variation in the literature is usually represented in relative values to mean instead of absolute values. In this work we refer to the diurnal variation represented in relative values as simply "diurnal variation."

2. GEC Models and Approaches

In this section 2 we describe all modeling approaches used in this work and corresponding results are summarized in Table 1. First, in section 2.1, two GEC models using current dipoles to represent thunderstorms (RBF and FVS) are described. These models are applied in section 3.1 for evaluation of resistance of atmosphere, which is a first necessary step before evaluation of ionospheric potential. In section 3.2, GEC model

Table 1
Maxima and Minima of Diurnal Variations for Results Shown in Figures 2 (FVS-ϕ) and 3 (Others)

	Minimum		Maximum		
Model	Peak	Time	Peak	Time	Description
Burns et al. (2012)-E	86%	4:00	119%	19:30	Direct measurements
TRMM-MEAN-I	86%	3:00	110%	14:00	Land/ocean storm counts
TRMM-PMO-I	84%	4:00	117%	20:00	Microwave observations
Mach et al. (2011)-I	77%	4:30	119%	20:30	Land/ocean storm counts
CESM-I	91%	4:00	106%	15:00	Convective mass flux from CESM
CESM-E	90%	4:00	108%	14:00	Using CESM (WACCM-GEC model)
FVS-ϕ (Figure 2, CESM σ)	90%	3:00	110%	21:00	Using TRMM-MEAN-I and CESM σ

Note. Diurnal variations based on last letter of model label are: "E" represents field on ground at Vostok, "I" represents the source current parameterizations, and "ϕ" represents ionospheric potential variation. The table is structured to present direct measurements first, current parameterizations second, and GEC models third.

FVS is used with realistic current and conductivity distributions to study the effect of realistic conductivity on diurnal variation of ionospheric potential (FVS-ϕ).

Second, in section 2.2 the methods using the current above thunderstorms are described. Section 2.2.1 covers the current parameterization derived from mean thunderstorm currents obtained from plane overflights combined with global TRMM satellite data on thunderstorm distribution (TRMM-MEAN-I), and current parameterization derived from passive microwave observations from plane overflights combined with global TRMM satellite data of passive microwave observations (TRMM-PMO-I). These results are presented in section 3.3.2. Section 2.2.2 describes the use of GEC model within global circulation model CESM. Two data sets are produced and presented in section 3.3.1: current distribution above the thunderstorms (labeled CESM-I) and electric field on the ground at Vostok location (labeled CESM-E).

2.1. GEC Models Using Current Dipoles

We use two three-dimensional spherical models $(r,\ \theta,\ \varphi)$ to represent electrical behavior of the GEC. First, the model based on radial basis functions is described in (Bayona et al., 2015; Fornberg & Flyer, 2015) and is referred to as RBF in this work. Second, a model based on a finite volume method on a structured mesh is described in Jánský and Pasko (2014) and is referred to as FVS. The models are based on the steady state current continuity equation for current density $\vec{j}$:

$$\vec{\nabla} \cdot \vec{j} = S_{\text{cur}}\,, \tag{1}$$

where current density $\vec{j} = \sigma \vec{E}$ is the product of electric field $\vec{E}$ and conductivity σ and the quantity S_{cur} represents the current source term. In both models, equation (1) is solved for unknown electric potential ϕ ($\vec{\nabla}\phi = -\vec{E}$), which is also used for boundary conditions described later in this section.

The schematics of the simulation domain are shown in Figure 1a. The domain is bounded by two conductive spherical layers with Dirichlet boundary conditions for potential. The potential on Earth's surface at $r_{\text{Earth}} = 6,371$ km is set to $\phi_{\text{Earth}} = 0$ V. The top boundary of the computational domain is referred to in this work as top ionospheric boundary (TIB) and is set at altitude $h_{\text{TIB}} = 60$ km in RBF model and 55.2 km in FVS model, and its potential ϕ_{TIB} is set depending on the considered model case, see end of section 2.1 for more details. In GEC framework this boundary should not be confused with altitude range of the Earth ionosphere that extends to higher altitudes. In GEC this boundary is referred to altitude where conducting medium can be treated with high accuracy as equipotential (Jánský & Pasko, 2014). Ionospheric potential is defined as the potential difference between TIB and Earth: $\phi_{\text{IE}} = \phi_{\text{TIB}} - \phi_{\text{Earth}}$.

The model developed by Bayona et al. (2015) is used with the radial coordinate split into 120 nodes with a stretching constant 0.05 and a horizontal resolution of 1.5° in latitude and longitude. The model developed in Jánský and Pasko (2014) is a time-dependent model that includes a conducting Earth as part of the simulation domain. For the purpose of this paper, the boundary conditions are adjusted as described above and shown in Figure 1a. Equation (1) is solved using finite volume method and the direct solver MUMPS (Amestoy et al., 2001) analogously to the solution of Poisson's equation described in Jánský and Pasko (2014). A structured

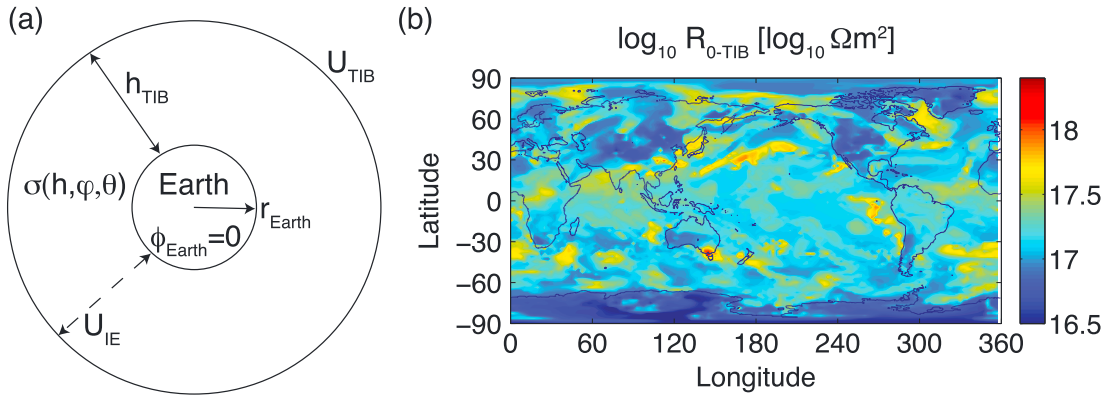

Figure 1. (a) Schematics of the computational domain. Full view on Earth and top ionospheric boundary (TIB) drawn not to scale. (b) Decimal logarithm of columnar resistance ($\log_{10}\Omega\,m^2$) between Earth and top ionospheric boundary as a function of longitude and latitude.

mesh is used with 144 cells in the longitudinal direction and 95 in the latitudinal direction, utilizing the same horizontal grid used for the conductivity calculations in CESM. In the radial direction, 40 points with a mesh step of 0.25 km are used to describe the bottom of the atmosphere and then the mesh step expands with a factor 1.1 with increasing altitude. In total 70 points in the radial direction are used.

In the altitude range from 0 to 60–70 km the lower and upper boundaries can be considered as perfect conductors (Dejnakarintra & Park, 1974). Conductivity in this range is isotropic (e.g., Dejnakarintra & Park, 1974, Figures 4a and 4b). Three choices of conductivity, σ, are used in this work. The first one is an exponential approximation (e.g., Dejnakarintra & Park, 1974):

$$\sigma(h) = 5 \times 10^{-14} \exp(h/l)\,\mathrm{S\,m^{-1}}, \tag{2}$$

where h is altitude and $l = 6$ km is the altitude scaling distance. The second one is the yearly average of conductivity obtained from the global circulation model CESM. We use the stand-alone atmospheric component configuration with the Community Atmosphere Model (CAM5) extended to the Whole Atmosphere Community Climate Model (WACCM). Conductivity reduction for nonelectrified clouds is estimated to range from 1/10 (Nicoll & Harrison, 2009) to 1/50 (Zhou & Tinsley, 2010). The value 1/50 is selected in CESM simulations for consistency with previous work (Baumgaertner et al., 2014). The columnar resistance (Baumgaertner et al., 2013, equation (10)) as a function of latitude and longitude is shown in Figure 1b. The CESM is free running with a time step of 30 min, a resolution of 2.5° in longitude and 1.9° in latitude, with 70 vertical levels distributed in modified pressure coordinates, which correspond to roughly 140 km as the top height. Only 51 levels up to roughly 70 km are used for conductivity calculation. The conductivity module of CESM is developed and described in Baumgaertner et al. (2013, 2014). The yearly average conductivity is calculated from time resolved conductivity $\sigma(t)$ as the harmonic mean value over the years 2005–2007:

$$\bar{\sigma} = \frac{N}{\sum_{N} \frac{1}{\sigma(t)}}, \tag{3}$$

where N represents the number of time steps over the years 2005–2007. This equation can be interpreted as the mean value for resistivity ($\sim 1/\sigma$) and is an appropriate representation of the total resistance of the atmosphere as will be described in section 3.1. The conductivity from CESM includes topography (elevated regions lead to drop in atmospheric resistance), ^{222}Rn ionization (increase in ionization above ground leads to drop in atmospheric resistance), aerosols, and clouds (decrease of conductivity due to attachment to large particles leads to increase of atmospheric resistance). The current convergence/divergence around fair-weather clouds developed in Baumgaertner et al. (2014) is also included. Years 2005–2007 are selected to include the year 2005, which was used to evaluate the current parameterization (Kalb et al., 2016) with the model CESM. Three year range is selected to minimize the effect of interannual variation.

To separate out the effects of clouds, the conductivity without clouds is also used for the study of the diurnal variation (Baumgaertner et al., 2013, Figure 7a). This conductivity profile includes ^{222}Rn ionization, aerosols, and topography. It is important to note that the treatment of clouds in CESM has advanced since

Baumgaertner et al. (2013) and that is why the conductivity profile with clouds is simulated again from CESM instead of adopting data from Baumgaertner et al. (2013, Figure 7b).

The source term, S_{cur}, is input as a current dipole representing the contribution of electrified clouds. The exact distribution of altitudes for current dipoles over Earth is not available, and therefore, for this work altitudes of the current dipoles, $I_s = S_{cur}\, V_s$, are assumed to be 4.5 km for all bottom negative charge centers of the electrified clouds and 9.5 km for all of the top positive charge centers, similarly to Jánský and Pasko (2014). V_s is the volume of each pole consisting of two cells in the computational domain. One cell is placed above the other forming a current monopole from 9.25 km to 9.75 km for the top pole. The distribution of the amplitudes of the current dipoles, I_s, is assumed to be proportional to the TRMM-MEAN-I, global distribution of current density at 20 km obtained from the TRMM mission (Kalb et al., 2014) which is further described in section 2.2.1. The constant of proportionality is selected arbitrarily as it has no effect on the diurnal variation, which, as already noted in section 1 is represented in relative values. This distribution provides time (1 h) and space (1°) representation of electrified clouds.

The computational strategy and equations described in Bayona et al. (2015, section 2) are used to solve equation (1) in both RBF and FVS models. Briefly, first the resistance of the atmosphere R_a between two conductive layers (Earth and TIB) is evaluated by imposing unit value $\phi_{TIB} = \phi^0 = 1$ V and a domain free of sources $S_{cur} = 0$. Having denoted the solution of equation (1) for these conditions as $\vec{j}_f$ and using Ohm's law, we obtain

$$R_a = \frac{\phi_{TIB}}{I_f}, \quad I_f = -\oiint_{TIB} \vec{j}_f \cdot \mathrm{d}\vec{S}, \tag{4}$$

where I_f denotes the downward directed current flowing between the Earth and TIB only due to the potential difference 1 V. The resistances obtained from different models are compared in section 3.1.

The second step consists of evaluation of currents flowing upward to the TIB in the domain due to the electrified clouds, current sources represented by dipoles. S_{cur} is therefore included and represents the dipole contribution (Bayona et al., 2015, section 4.6.1). Potential of the TIB is set to $\phi_{TIB} = 0$ V as only in this case the linear combination of solutions in both steps leads to the correct solution of the complete system. The upward current I_u flowing to the TIB due to dipoles is obtained from solution of equation (1) for these conditions $\vec{j}_u$:

$$I_u = \oiint_{TIB} \vec{j}_u \cdot \mathrm{d}\vec{S}. \tag{5}$$

The ionospheric potential for the combined system is then $\phi_{IE} = R_a\, I_u$ and current density is obtained by linearly combining $\vec{j} = \vec{j}_u + R_a\, I_u / 1\,\mathrm{V}\, \vec{j}_f$. It is important to note that current density $\vec{j}$ provides a solution with balanced zero total current at TIB I_{TIB}:

$$I_{TIB} = \oiint_{TIB} \vec{j} \cdot \mathrm{d}\vec{S} = 0. \tag{6}$$

2.2. GEC Models Using Current Above the Storm

2.2.1. Methods to Obtain the Current Above the Storm

An alternative method of obtaining current flowing upward to the TIB, I_u, without solving equation (1), uses the knowledge of the global distribution of current density at 20 km produced from thunderstorms and electrified shower clouds (Bayona et al., 2015, section 4.6.2). Then the integral of the global distribution of current density at 20 km is equal to I_u.

Kalb et al. (2014) obtained the global distribution of current density at 20 km by analyzing TRMM observations. Global total storm current distributions were computed from a precipitation and cloud feature database employed in Liu et al. (2010), which is based on TRMM observations. This database contains counts of thunderstorms and electrified shower clouds in 1° grid boxes between 35° south and 35° north latitudes. Using the Liu et al. (2008) database, currents were first estimated by multiplying the Mach et al. (2010) mean current values of 1.7 A for thunderstorms and 0.41 A for electrified shower clouds with the counts of thunderstorms and electrified shower clouds over oceans from Liu et al. (2010). Also, the mean current values of 1.0 A and 0.13 A were multiplied with the thunderstorm and electrified shower clouds over land. This methodology produced a total current estimate of 1609 A. This value is more akin to the global current estimate of 1400 A

(Kraakevik, 1961), yet it covers only the tropical and subtropical latitudes. Therefore, rare events with large currents were removed from the current database to improve agreement, and new means computed. These new means of 1.17 and 0.41 A for thunderstorms and electrified shower clouds over oceans, and 0.21 and 0.08 A over land (Kalb et al., 2016) were multiplied by the storm counts to produce a total current for each grid box. This current is referred to as the TRMM derived current in present work and is abbreviated as TRMM-MEAN-I. It has a 1 h diurnal resolution and is also used in section 3.2 as the current source for the FVS method.

Peterson et al. (2015) developed an algorithm that leverages ice-scattering signals from 37 and 85 GHz passive microwave observations to estimate the electric fields above electrified clouds at 20 km altitude. The basic assumption of the algorithm is that cloud ice processes are the primary source of cloud charge. The amount of charge generated should be a function of the frequency of collisions between ice particles, which depends in part on the amount of ice in the cloud (Peterson et al., 2015). It was developed using a collocated passive microwave and electric field data set produced from NASA ER-2 measurements and is shown to estimate observed electric field strengths over intense convective clouds at least 71% (58%) of the time over land and 43% (40%) of the time over the ocean to within a factor of 2 from 85 GHz (37 GHz) passive microwave observations. Peterson et al. (2017) applied this algorithm to globally measured ice-scattering signals from 85 GHz using the TRMM satellite to obtain a global current distribution. The currents presented in this work are computed at 20 km to compare with the other methods. Only the contribution of convective electrified clouds is considered. The total contribution of stratiform clouds is assumed to be small. This assumption is further discussed in section 4. Current distribution obtained from this method is referred to as TRMM-PMO-I in this work.

The TRMM satellite has a non-Sun-synchronous 35° inclination orbit covering the tropics and subtropics, with instruments for observing precipitation, clouds, and lightning (Kummerow et al., 1998). Given enough observation time, TRMM data provide detailed information about the diurnal cycles of precipitation and clouds (Liu et al., 2010) and is representative for annual average of diurnal variation.

2.2.2. Methods Using the Global Circulation Model CESM

Kalb et al. (2016) developed a parameterization of current above storms using the convective mass flux, which is a variable that can be obtained from models like CESM. Yearly averaged convective mass flux is first multiplied by the grid box area and integrated to isolate the mixed phase region of clouds, defined to be between 0 and −50°C. Then, the data are binned, and the mean value within each bin is compared to the mean TRMM derived current (TRMM-MEAN-I) in each bin. A power law relationship is fitted to the binned data, separately for land and ocean data, as we would expect that the land and ocean regimes may have different relationships. The parameterization was derived using CESM data from the year 2005. This current, obtained by applying parameterization of Kalb et al. (2016) to CESM for the years 2005–2007, is referred to as CESM-I in this work.

Lucas et al. (2015) developed a modeling framework of the GEC for use within the global circulation models, specifically CESM, called WACCM-GEC. Both source current and conductivity are obtained from CESM. In this work, compared to Lucas et al. (2015), the CESM with improved source current parametrization (Kalb et al., 2016) is used and the diurnal variation is evaluated as the mean value over the years 2005–2007. It is important to note that CESM-I and CESM-E are obtained from the same simulation run of CESM. For analysis, the fair-weather electric field at Vostok is obtained from this model (Lucas et al., 2015, equations (5)–(7)) and is referred to as CESM-E in this work. The model is based on an equivalent circuit description of the fair-weather part of the GEC, which neglects the small horizontal currents. For a horizontally coarse mesh used in CESM this assumption is appropriate and speeds up the simulations significantly compared to 3-D GEC models.

3. Results

3.1. Resistance of the Atmosphere

The ionospheric potential based on computational strategy described in section 2.1 is solved in two steps. First step consists of evaluating the resistance of the atmosphere R_a based on equation (4). It was found that for arbitrary conductivity profile taken from CESM, FVS and RBF numerical models do not yield consistent resistances due to mesh differences and interpolation. Therefore, it is necessary to achieve convergent results from FVS and RBF models before advancing to second step of solution for ionospheric potential.

In this section the resistance of atmosphere is calculated using the FVS and RBF models, and additionally, the analytic representation of resistance

$$R = \left[\int_0^{2\pi} \int_0^{\pi} \left(\int_{\text{surface}}^{60\,\text{km}} \frac{\mathrm{d}r}{\sigma r^2} \right)^{-1} \sin\theta \, \mathrm{d}\theta \, \mathrm{d}\varphi \right]^{-1} \tag{7}$$

is used for comparison. The resistance obtained from equation (7) is referred to as the integral approach in the discussion that follows. Note that compared to the approach described in Baumgaertner et al. (2013, equations (10) and (11)), we incorporate the radial coordinate, r, as a variable instead of setting it equal to the radius of the Earth, r_{Earth}. The two cases of conductivity are compared. The first is using exponential conductivity, see equation (2), and the second corresponds to the yearly average of conductivity obtained from CESM for conditions including topography, ^{222}Rn ionization, aerosols, and clouds. It is important to add that the analysis of topography influence with exponential conductivity profile on atmospheric resistance was performed by Bayona et al. (2015). It was found that including Earth topography compared to the spherical Earth's surface decreases the atmospheric resistance by 10 Ω.

For an exponential conductivity profile the GEC models have to converge to the same result as the integral approach (see discussion in Jánský & Pasko, 2015, section 3.1). The integral approach is solved analytically, and 234.8 Ω is obtained. For the meshes described in section 2.1, the FVS model gives 234.9 Ω and the RBF model gives 235.4 Ω. Both of the models agree within an accuracy of 0.3%. Additional convergence studies performed using finer meshes with both models proved their validity and converged to 234.8 Ω.

For the yearly averaged conductivity obtained from CESM: FVS gives 274 Ω, RBF gives 267 Ω, and the numerical integral approach gives 279 Ω. These values agree well with the annual mean resistance 285 Ω obtained from CESM for similar conditions with same cloud conductivity reduction $\eta = 1/50$ (Baumgaertner et al., 2014, Table 1). Available values of atmospheric resistance in literature range from 110 to 300 Ω depending on considered assumptions (Baumgaertner et al., 2014; Zhou & Tinsley, 2010). For validation purposes the resistance is compared only with the closest approach of Baumgaertner et al. (2014). It is important to note that using the arithmetic mean value instead of the harmonic mean in equation (3) leads to a significantly lower resistance of ∼210 Ω. The FVS, RBF, and the integral approach agree within 4%, which is considered a very good agreement. The difference can be attributed to the following reasons. The FVS and RBF models both introduce error through interpolation of conductivity onto their meshes. The integral approach follows the mesh but as the horizontal variations of conductivity introduce small horizontal currents, which are neglected by integral approach, resistance is higher compared to the resistances obtained from the 3-D GEC models. It is important to note that if the conductivity from CESM is taken for a given time step instead of averaged conductivity over multiple time steps using equation (3), the conductivity profiles are less smooth producing higher interpolation errors and higher resistance differences. In related studies (not shown here for the sake of brevity) differences up to 20% were observed when using individual time step data within the 3-D solving models due to large "jumps" in conductivity between mesh points.

In conclusion, the conductivity profiles obtained from CESM and processed using equation (3) provide convergent resistances of atmosphere and can be used for analysis of the GEC using the 3-D GEC models. In the next section, only FVS model is used to study diurnal variation as RBF model would provide the same results.

3.2. Diurnal Variation of Ionospheric Potential for Different Conductivities

In this section, the FVS model is used to study the influence of conductivity on the diurnal variation of the ionospheric potential of the GEC. Ionospheric potential is found to be an important quantity, which can serve as a global indicator relating the state of global electric circuit (GEC) to the planetary climate (e.g., Williams & Mareev, 2014, section 10). The diurnal variation of ionospheric potential is proportional to diurnal variation of current sources with constant of proportionality being atmospheric resistance (see section 2.1). The electrified clouds are represented by dipoles according to the size, altitudes and source currents described in section 2.1. The annual harmonic mean of conductivity from CESM, equation (3), is used.

The diurnal variation of the ionospheric potential, ϕ_{IE}, of the GEC is shown in Figure 2a. First, the diurnal variation of ionospheric potential ϕ_{IE} with exponential conductivity, shown as the blue full curve, is the same as the diurnal variation of the source current, TRMM-MEAN-I in this case. Second, the diurnal variation with conductivity obtained from CESM, shown as the red dashed curve, decreases the first maximum at 14 UT from

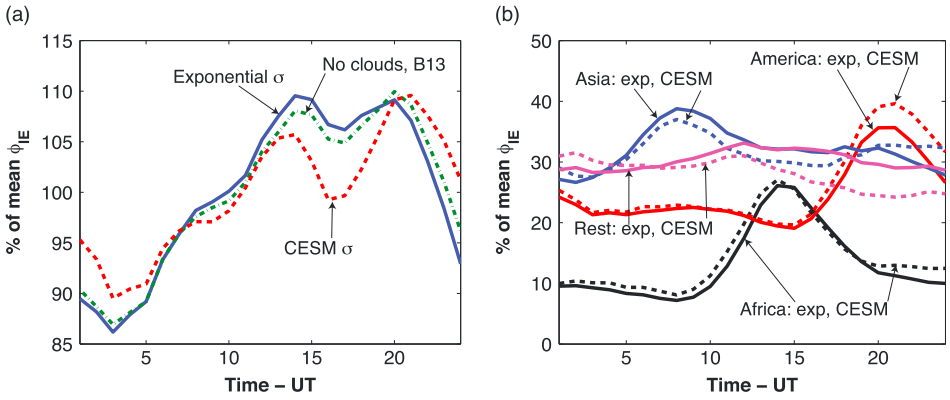

Figure 2. (a) Diurnal variation of ionospheric potential obtained from FVS model with current sources based on TRMM-MEAN-I for three cases with different conductivity: exponential shown as blue solid curve, conductivity without clouds (Baumgaertner et al., 2013) shown as green dash-dotted curve (No clouds, B13), and conductivity from CESM including clouds shown as red dashed curve (CESM σ). (b) Diurnal variation of ionospheric potential for exponential conductivity (solid curves) and conductivity from CESM including clouds (dashed curves) for four areas of Earth. Areas are defined by longitude intervals and are labeled by major contributing area: Africa 0°:60° (black curves), Asia 90°:180° (blue curves), America 240°:330° (red curves), and Rest corresponds to rest of the world (purple curves).

110% to 106%, increases the second maximum at 21 UT from 109% to 110%, and increases the minimum at 3 UT from 86% to 90%. The peak to peak diurnal variation is therefore decreased from 24% to 20%. The diurnal variation is split into contributions from geographic areas to identify the influence of each area on the diurnal variation. The data for both exponential and CESM conductivity are shown as solid curve and as dashed curve in Figure 2b, respectively. Geographic areas are defined by longitude intervals and are labeled by major contributing area: Africa 0°:60°, Asia 90°:180°, America 240°:330°, and Rest corresponds to the rest of the world. It is seen that with the conductivity from CESM the relative contribution of America, shown as red curves, is increased around 20 UT. Africa's contribution, shown as black curves, remains the same over the whole day. Asia's contribution, shown as blue curves, is slightly decreased from its peak at 8 UT until 20 UT. The rest of the world, shown as purple curves, is decreased in particular after 12 UT.

The interpretation of the behavior observed in Figure 2 is not straightforward. The conductivity influences ionospheric potential proportionally to ratio of columnar resistance between the bottom negative (BN) and top positive (TP) charge centers, $R_{\text{BN-TP}}$, to the columnar resistance from the earth surface to TIB, $R_{\text{0-TIB}}$: $\phi_{IE} \sim I_s R_{\text{BN-TP}}/R_{\text{0-TIB}}$ (e.g., Jánský & Pasko, 2015). The variation of columnar resistances has significant random component due to the distribution of clouds seen in Figure 1b. Therefore, the conductivity profile without clouds is used to separate out the influence due to clouds (Baumgaertner et al., 2013, Figure 7a). The diurnal variation using the conductivity profile that includes ^{222}Rn ionization, aerosols, and topography but no clouds is shown as green dash-dotted curve in Figure 2a and is closer to the case with exponential conductivity than to the case with clouds. It is seen that the combined presence of the above mentioned factors increases the diurnal variation after 20 UT from 109% to 110%, while around 15 UT it is decreased from 110% to 108%. The peak to peak diurnal variation is decreased from 24% to 23%.

In conclusion, the peak to peak diurnal variation is decreased from 24% to 20% by including the conductivity profile from CESM. The main reason for the change is the presence of clouds. If clouds are removed, the peak to peak diurnal variation is decreased from 24% to 23% by including ^{222}Rn ionization, aerosols, and topography. We note that clouds in CESM reproduce both the observed total cloud cover and the regional distribution measured by satellites very well (Baumgaertner et al., 2014, and references therein). It is important to mention that in this analysis the yearly averaged data are used for both current sources and conductivity. The current sources and conductivity vary on shorter timescales in the GEC, and therefore, with better time refined analysis the related variability is expected to be observable.

3.3. Comparison of Diurnal Variations

3.3.1. Methods Using the Global Circulation Model CESM

This section compares the annual average of relative diurnal variation obtained from the models and data sets relevant to CESM described in sections 2.2.1 and 2.2.2 with experimental measurements from Vostok station in Antarctica (Burns et al., 2012, Figure 12c). It is important to note that Burns et al. (2012) used the

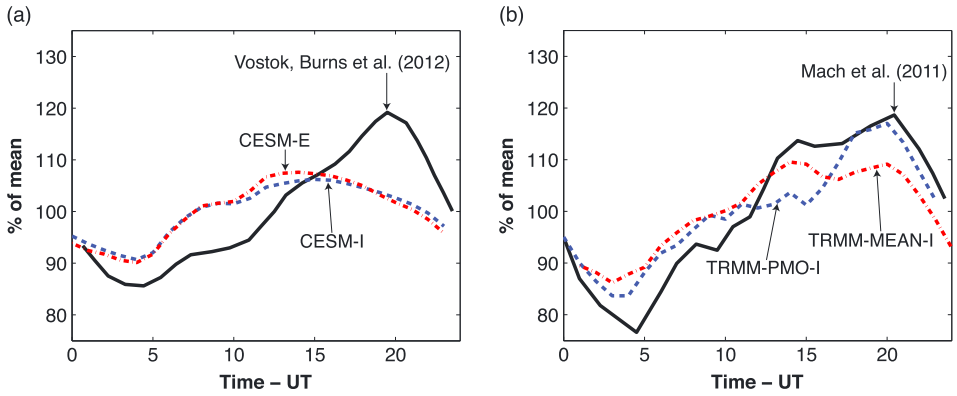

Figure 3. (a) Comparison of diurnal variation for results related to CESM climate model, CESM-I (blue dashed curve) and CESM-E (red dash-dotted curve), with experimental data(Burns et al., 2012) (black solid curve). (b) Comparison of diurnal variation of global currents in GEC obtained by methods using global satellite measurements combined with overflights: TRMM-MEAN-I (red dash-dotted curve), TRMM-PMO-I (blue dashed curve), and data from(Mach et al., 2011) (black solid curve). The description of abbreviations and methods is available in section 2.2.

Weimer model (Weimer, 1995) to calculate the solar wind imposed contribution to ground potential difference above Vostok and subtracted it from their experimental results of the annual diurnal curve to obtain the electric field used for comparison in present work (Burns et al., 2012 Figure 12c). The comparison is shown in Figure 3a, and peak values are summarized in Table 1. CESM-I (blue dashed curve) and CESM-E (red dash-dotted curve) produce a global current that flows in the GEC and a surface electric field at Vostok, respectively. Both methods related to CESM produce similar results. The minimum value of the diurnal variation is 91% for CESM-I and 90% for CESM-E compared to 86% measured at Vostok, shown as black solid curve. At the maximum of the diurnal variation CESM-I gives 106% and CESM-E gives 108% compared to 119% at Vostok. The CESM related diurnal variations have also their maximum earlier at 14 and 15 UT than the measured one at Vostok at 19:30 UT. It is also important to note that the difference between CESM-I and CESM-E results from the transformation of global current flowing in the GEC (CESM-I) to the ionospheric potential, which then manifests itself in the electric field modeled at Vostok (CESM-E). This transformation is a function of the conductivity profile of atmosphere (Lucas et al., 2015, equations (5)–(7)). It can be concluded that the conductivity profile from CESM increases peak to peak diurnal variation from 15% to 18% due to the effect of transformation of the global current in the GEC to the field at Vostok.

3.3.2. Methods to Obtain Current Above the Storm

The relative diurnal variations of results obtained using parameterizations combined with satellite data are shown in Figure 3b and peak values are summarized in Table 1. The data TRMM-MEAN-I (red dash-dotted curve) and TRMM-PMO-I (blue dashed curve) are described in section 2.2.1. The data calculated by Mach et al. (2011) are shown as black solid curve for comparison as they represent the best agreement with Vostok observations that can be found in literature. All data are composed of a global current, I_u, flowing in the GEC due to electrified clouds. TRMM-MEAN-I has a minimum of 86% at 3 UT, a global maximum of 110% at 14 UT and a local maximum of 109% at 20 UT. TRMM-PMO-I has a minimum of 84% at 4 UT and a maximum of 117% at 20 UT. Mach et al. (2011) calculated a diurnal variation with a minimum of 77% at 4:30 UT, global maximum of 119% at 20:30 UT and local maximum of 114% at 14:30 UT. It is seen that TRMM-PMO-I gives the best agreement with measured values at Vostok (Burns et al., 2012). The discussion of these results follows in the next section 4.

4. Discussion

This section discusses of the influence of TRMM satellite range, the uncertainty in electrified shower cloud counts, the time and space resolution of conductivity obtained from CESM, and the small influence of stratiform clouds in approach using passive microwave observations.

First we discuss the influence of the TRMM satellite range, as the satellite only collects data between the latitudes [−35°:35°] due to the orbital inclination of the satellite. Having considered CESM-I currents that are integrated only between latitudes [−35°:35], the relative diurnal variation has the same shape as CESM-I

integrated over the entire Earth, but the minimum is decreased from 92% to 87% and the maximum is increased from 106% to 110%. It is important to note that the data set TRMM-MEAN-I, which is obtained between the latitudes [−35°:35°] is used as a reference in CESM-I and that these new peak values agree very well with TRMM-MEAN-I peak values. Therefore, it can be concluded that the parameterization developed by Kalb et al. (2016) is working well and the global reference TRMM-MEAN-I data set is responsible for the difference of CESM based models in comparison with the experimental measurements. More detailed discussion of the CESM-I currents can be found in Kalb et al. (2016).

TRMM-MEAN-I data set is obtained using a precipitation and cloud feature database from (Liu et al., 2010), which is based on TRMM observations. The storm and electrified shower cloud counts are multiplied by mean currents above them to obtain the global current. The mean currents are derived from 850 overflights around North America and Australia (Kalb et al., 2016). It is interesting to note that the data presented in Mach et al. (2011) are based on the same set of overflights, although the mean currents are different, as Kalb et al. (2016) improved them by removing outliers. The influence of the global distribution of electrified clouds on diurnal variation has been discussed by Mach et al. (2011). Mach et al. (2011) pointed out that their count of electrified shower clouds is smaller than in (Liu et al., 2010) and demonstrated that an increase in counts of electrified shower clouds leads to a decrease in amplitudes of the relative diurnal variation (Mach et al., 2011, Figure 13). This explains the differences observed between TRMM-MEAN-I and Mach et al. (2011) in Figure 3b. It is also important to consider that overflights used for the determination of mean currents were local in nature and generally covered the America's region. If mean currents vary globally over the different areas of Earth, the diurnal variation would be modified accordingly.

The results in section 3.2 show that the spatial variation of conductivity obtained from CESM modifies the diurnal variation of the ionospheric potential and consequently the global upward current I_u. In particular, the peak at 20 UT corresponding to activity in the Americas, where overflight measurements were performed, is increased. This suggests that the mean currents can be modified by the conductivity distribution in different areas of Earth. However, it was shown that the significant modification is caused by clouds. Clouds' distribution in CESM is resolved with a very coarse mesh (hundreds of kilometers) relatively to the size of a single electrified cloud (tens of kilometers). Therefore, it is possible that conductivity values used in this work do not accurately represent the GEC behavior, and a better spatial accuracy may produce a better agreement.

The TRMM-PMO-I data set provides the best comparison with the experimental curve obtained at Vostok in both time and peak value of maximum and minimum. TRMM-PMO-I uses globally measured ice-scattering signals at 85 GHz using the TRMM satellite to obtain a global current distribution instead of storm counts. The results for convective electrified clouds are presented and the effect of stratiform clouds is neglected. It is because the model assumes a convective charge structure which may not represent well the amplitudes of stratiform currents. The second reason is that stratiform clouds are often of inverted polarity (Williams & Mareev, 2014, section 3), and therefore, their total contribution to GEC cannot be represented using this approach. More detailed discussion of the TRMM-K16 currents can be found in Peterson et al. (2017).

5. Conclusions

We have analyzed the diurnal variation of the global electric circuit (GEC) using different numerical models. The principal results of this paper are as follows:

1. The two GEC three-dimensional models (labeled as RBF and FVS) are tested by solving for the fundamental parameter of total global resistance within the GEC. The models agree with analytical results within an accuracy of 0.3% for exponential conductivity. For conductivity obtained from the global circulation model CESM, both models and columnar integration of conductivity agree within accuracy of 4%. The importance of using a harmonic mean time averaging of conductivity and implementing smooth profiles to guarantee good accuracy is emphasized.
2. The peak to peak diurnal variation of the ionospheric potential of the GEC decreases from 24% to 20% if the exponential conductivity is substituted by the conductivity from the global circulation model CESM. The main reason for the change is the presence of clouds. If clouds are neglected, the peak to peak diurnal variation decreases from 24% to only 23% by including ^{222}Rn ionization, aerosols, and topography.
3. The simulated peak to peak diurnal variation of the electric field at Vostok, where reference experimental measurements are performed, increases from 15% to 18% from the diurnal variation of the global current in the GEC if conductivity from the global circulation model CESM is used.

4. The diurnal variations of the results obtained using local measurements from plane overflights combined with global satellite data give generally good agreement with experimental measurements at Vostok. It is observed that a combination of mean currents obtained from plane overflights at 20 km with global counts of electrified clouds provides reasonable diurnal variations. However, the uncertainty in the count of electrified shower clouds can still lead to differences in amplitudes. An alternative approach using passive microwave observations instead of electrified cloud counts is compared and shows the best agreement in amplitude and phase with experimental measurements.

Acknowledgments
This research was supported by NSF under grant AGS-1135446. CESM can be obtained through http://www.cesm.ucar.edu. RBF model is available at https://bitbucket.org/vbayona/gec_rbffd. FVS model is fully described in cited references. All data representing figures, current sources, and conductivity profiles used for simulations are available at https://doi.org/10.18113/D3395B.

References

Amestoy, P. R., Duff, I., L'Excellent, J., & Koster, J. (2001). A fully asynchronous multifrontal solver using distributed dynamic scheduling. *SIAM Journal on Matrix Analysis and Applications*, *23*(1), 15–41. https://doi.org/10.1137/S0895479899358194

Aplin, K. L., Harrison, R. G., & Rycroft, M. J. (2008). Investigating Earth's atmospheric electricity: A role model for planetary studies. *Space Science Reviews*, *137*(1–4), 11–27. https://doi.org/10.1007/s11214-008-9372-x

Bailey, J. C., Blakeslee, R. J., Buechler, D. E., & Christian, H. J. (2007). Diurnal lightning distributions as observed by the Optical Transient Detector (OTD) and the Lightning Imaging Sensor (LIS). In *Proceedings of the 13th International Conference on Atmospheric Electricity*. Beijing, China.

Baumgaertner, A. J. G., Thayer, J. P., Neely, R. R., & Lucas III, G. (2013). Toward a comprehensive global electric circuit model: Atmospheric conductivity and its variability in CESM1(WACCM) model simulations. *Journal of Geophysical Research: Atmospheres*, *118*, 9221–9232. https://doi.org/10.1002/jgrd.50725

Baumgaertner, A. J. G., Lucas, G. M., Thayer, J. P., & Mallios, S. A. (2014). On the role of clouds in the fair weather part of the global electric circuit. *Atmospheric Chemical Physics*, *14*(16), 8599–8610. https://doi.org/10.5194/acp-14-8599-2014

Bayona, V., Flyer, N., Baumgaertner, A. J. G., & Lucas, G. M. (2015). A 3-D RBF-FD solver for modeling the atmospheric global electric circuit with topography (GEC-RBFFD v1.0). *Geoscientific Model Development*, *8*, 3007–3020. https://doi.org/10.5194/gmd-8-3007-2015

Burns, G. B., Frank-Kamenetsky, A., Tinsley, B. A., French, W. J. R., Grigioni, P., Camporeale, G., & Bering, E. A. (2015). The global atmospheric circuit from Antarctic Plateau electric field measurements at Vostok and Concordia. *Abstracts of the 26th IUGG general assembly, Prague, Czech Republic, June 22 – July 2, 2015*.

Burns, G. B., Tinsley, B. A., Frank-Kamenetsky, A. V., Troshichev, O. A., French, W. J. R., & Klekociuk, A. R. (2012). Monthly diurnal global atmospheric circuit estimates derived from Vostok electric field measurements adjusted for local meteorological and solar wind influences. *Journal of the Atmospheric Sciences*, *69*(6), 2061–2082. https://doi.org/10.1175/JAS-D-11-0212.1

Dejnakarintra, M., & Park, C. G. (1974). Lightning-induced electric-fields in ionosphere. *Journal of Geophysical Research*, *79*(13), 1903–1910. https://doi.org/10.1029/JA079i013p01903

Fornberg, B., & Flyer, N. (2015). *A primer on radial basis functions with applications to the geosciences* (Vol. 87). Philadelphia, PA: SIAM.

Harrison, R. G. (2013). The Carnegie curve. *Surveys in Geophysics*, *34*(2), 209–232. https://doi.org/10.1007/s10712-012-9210-2

Jánský, J., & Pasko, V. P. (2014). Charge balance and ionospheric potential dynamics in time-dependent global electric circuit model. *Journal of Geophysical Research: Space Physics*, *119*, 10,184–10,203. https://doi.org/10.1002/2014JA020326

Jánský, J., & Pasko, V. P. (2015). Effects of conductivity perturbations in time-dependent global electric circuit model. *Journal of Geophysical Research: Space Physics*, *120*, 10,654–10,668. https://doi.org/10.1002/2015JA021604

Kalb, C., Wiebke, D., Baumgaertner, A., Mach, D., Liu, C., & Peterson, M. (2014). Parameterizing total storm conduction currents derived in a global model. In *Proceedings of the XV International Conference on Atmospheric Electricity*. Norman, OK.

Kalb, C., Deierling, W., Baumgaertner, A., Peterson, M., Liu, C., & Mach, D. (2016). Parameterizing total storm conduction currents in the Community Earth System Model. *Journal of Geophysical Research: Atmospheres*, *121*, 13,715–13,734. https://doi.org/10.1002/2016JD025376

Kalinin, A. V., Mareev, E. A., & Zhidkov, A. A. (2011). Calculation of different-type clouds in the global atmospheric electric circuit. In *Proceedings of the 14th International Conference on Atmospheric Electricity*. Rio de Janeiro, Brazil.

Kraakevik, J. (1961). Measurements of current density in the fair weather atmosphere. *Journal of Geophysical Research*, *66*(11), 3735–3748.

Kummerow, C., Barnes, W., Kozu, T., Shiue, J., & Simpson, J. (1998). The tropical rainfall measuring mission (TRMM) sensor package. *Journal of Atmospheric and Oceanic Technology*, *15*(3), 809–817.

Liu, C., Zipser, E. J., Cecil, D. J., Nesbitt, S. W., & Sherwood, S. (2008). A cloud and precipitation feature database from nine years of TRMM observations. *Journal of Applied Meteorology and Climatology*, *47*(10), 2712–2728.

Liu, C., Williams, E. R., Zipser, E. J., & Burns, G. (2010). Diurnal variations of global thunderstorms and electrified shower clouds and their contribution to the global electrical circuit. *Journal of the Atmospheric Sciences*, *67*(2), 309–323. https://doi.org/10.1175/2009JAS3248.1

Lucas, G. M., Baumgaertner, A. J. G., & Thayer, J. P. (2015). A global electric circuit model within a community climate model. *Journal of Geophysical Research: Atmospheres*, *120*, 12,054–12,066. https://doi.org/10.1002/2015JD023562

Mach, D. M., Blakeslee, R. J., Bateman, M. G., & Bailey, J. C. (2010). Comparisons of total currents based on storm location, polarity, and flash rates derived from high-altitude aircraft overflights. *Journal of Geophysical Research*, *115*, D03201. https://doi.org/10.1029/2009JD012240

Mach, D. M., Blakeslee, R. J., & Bateman, M. G. (2011). Global electric circuit implications of combined aircraft storm electric current measurements and satellite-based diurnal lightning statistics. *Journal of Geophysical Research*, *116*, D05201. https://doi.org/10.1029/2010JD014462

Mareev, E. A., & Volodin, E. M. (2014). Variation of the global electric circuit and ionospheric potential in a general circulation model. *Geophysical Research Letters*, *41*, 9009–9016. https://doi.org/10.1002/2014GL062352

Markson, R. (2007). The global circuit intensity: Its measurement and variation over the last 50 years. *Bulletin of the American Meteorological Society*, *88*(2), 223. https://doi.org/10.1175/BAMS-88-2-223

Nicoll, K. A., & Harrison, R. G. (2009). Vertical current flow through extensive layer clouds. *Journal of Atmospheric and Solar-Terrestrial Physics*, *71*(17), 2040–2046.

Peterson, M., Liu, C., Mach, D., Deierling, W., & Kalb, C. (2015). A method of estimating electric fields above electrified clouds from passive microwave observations. *Journal of Atmospheric and Oceanic Technology*, *32*(8), 1429–1446. https://doi.org/10.1175/JTECH-D-14-00119.1

Peterson, M., Deierling, W., Liu, C., Mach, D., & Kalb, C. (2017). A TRMM/GPM retrieval of the total mean generator current for the global electric circuit. *Journal of Geophysical Research: Atmospheres*, *122*, 10,025–10,049. https://doi.org/10.1002/2016JD026336

Weimer, D. (1995). Models of high-latitude electric potentials derived with a least error fit of spherical harmonic coefficients. *Journal of Geophysical Research*, *100*(A10), 19,595–19,607. https://doi.org/10.1029/95JA01755

Whipple, F. J. W. (1929). On the association of the diurnal variation of the electric potential gradient in fine weather with the distribution of thunderstorms over the globe. *Quarterly Journal of the Royal Meteorological Society*, *55*, 351–362. https://doi.org/10.1002/qj.49705523206

Whipple, F. J. W., & Scrase, F. J. (1936). Point-discharge in the electric field on the Earth. *Geophysical memoirs*, *8*(68), 1–20.

Williams, E., & Mareev, E. (2014). Recent progress on the global electrical circuit. *Atmospheric Research*, *135*, 208–227. https://doi.org/10.1016/j.atmosres.2013.05.015

Williams, E. R. (2009). The global electrical circuit: A review. *Atmospheric Research*, *91*(2-4, Sp. Iss. SI), 140–152. https://doi.org/10.1016/j.atmosres.2008.05.018.

Wilson, C. T. R. (1921). Investigations on lightning discharges and on the electric field of thunderstorms. *Philosophical Transactions of the Royal Society London A*, *221*, 73–115.

Zhou, L., & Tinsley, B. A. (2010). Global circuit model with clouds. *Journal of the Atmospheric Sciences*, *67*, 1143–1156. https://doi.org/10.1175/2009JAS3208.1